Impact of heat islands vs. city greening

Real-time monitoring and modeling of drinking water temperature in the city of Montreal in Canada

Absalan, Faezeh; Hatam, Fatemeh; Blokker, Mirjam; Besner, Marie Claude; Prévost, Michèle; Bichai, Françoise

DOI
10.1016/j.watres.2024.121490

Publication date
2024

Document Version
Final published version

Published in
Water Research

Citation (APA)
Absalan, F., Hatam, F., Blokker, M., Besner, M. C., Prévost, M., & Bichai, F. (2024). Impact of heat islands vs. city greening: Real-time monitoring and modeling of drinking water temperature in the city of Montreal in Canada. *Water Research*, *256*, Article 121490. https://doi.org/10.1016/j.watres.2024.121490

Water Research 256 (2024) 121490

Contents lists available at ScienceDirect

Water Research

journal homepage: www.elsevier.com/locate/watres

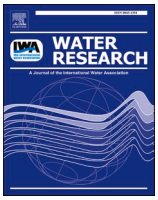

Impact of heat islands vs. city greening: Real-time monitoring and modeling of drinking water temperature in the city of Montreal in Canada

Faezeh Absalan [a,*], Fatemeh Hatam [a], Mirjam Blokker [b], Marie-Claude Besner [c], Michèle Prévost [a], Françoise Bichai [a]

[a] NSERC Industrial Chair in Drinking Water, Department of Civil, Geological and Mining Engineering, Polytechnique Montreal, CP 6079, Succ. Centre-ville, Montreal, QC H3C 3A7, Canada
[b] KWR Water Research Institute, Delft University of Technology, Groningenhaven 7, 3433 PE Nieuwegein, the Netherlands
[c] Water Services, City of Montréal, Montréal, QC H3C 0G4, Canada

ARTICLE INFO

Keywords:
Global warming
Urban heat island
Urban greening
Water temperature modeling
Water distribution network
Urban planning

ABSTRACT

Urbanization increases the land surface temperature through surface mineralization, adversely affecting vegetation and enhancing the urban heat island (UHI) effect. Global climate change has intensified this warming effect with more frequent and intense heatwaves during hot seasons. While these transformations influence soil temperature, their consequences on drinking water temperature within the drinking water distribution system (DWDS) remains poorly understood. Literature proposes to increase pipe burial depths to mitigate drinking water heating during summer. In this study, we monitored drinking water temperatures in a DWDS in Montreal, Canada with deeply buried pipes (average 1.8 m) during the summer of 2022, focusing on two contrasting zones in terms of UHI and green coverage. Monitoring revealed a 8°C heating effect compared to the water treatment plant, attributed to low green coverage and anthropogenic heat. Conversely, the greener zone exhibited cooler drinking water temperatures, reaching a maximum cooling effect of 8°C as compared to the temperature at the exit of the water treatment plant. Utilizing a soil and water temperature model, we predicted drinking water temperatures within the DWDS with acceptable accuracy. Soil temperature modeling results aligned well with measured water temperatures, highlighting DWDS water temperature approaching its surrounding soil temperature fairly quickly. Despite heatwaves, no immediate correlation emerged between air temperature records and measured water temperatures, emphasizing soil temperature as a superior indicator. An increase in water age displayed no correlation with an increase in measured water temperature, underscoring the dominant influence of UHI and green coverage on water temperature. These findings highlight the cooling advantages of green spaces during summer, providing valuable insights for sustainable urban planning.

1. Introduction

Urbanization is replacing natural land coverage with impervious surfaces, causing reduced evapotranspiration, increased heat capacity of the land surface and increased land surface temperature (LST) (Ranagalage et al., 2019; Wang et al., 2022). Elevated LSTs in cities due to natural global warming, urbanization, vegetation loss, and anthropogenic heat cause irregularities in urban energy balance and leads to creation of UHIs, increasing the local air, soil surface, and soil subsurface temperature (Estrada-Calderon and Becerra-Santacruz, 2022; Menberg et al., 2013). Alexander (2021) found that increasing the building heights and decreasing the vegetation height can increase the LST in cities. Zhu et al. (2021) studied the cooling effect of urban parks in Jinan, China, using Landsat 8 images and showed that the urban parks' LST is on average 3.6°C lower than its surrounding, with the most significant cooling effect of 7.8°C during summer days. Kafy et al. (2022) found a significant correlation between the vegetation loss and LST in the fast-growing city of Cumilla in Bangladesh. In 25 years, the city lost 9% of its vegetation cover due to urbanization, leading to a 11-°C increase in its average LST. Edan et al. (2021) studied the impact of land use/land cover change on LST from 2000 to 2020 in Al Kut, Iraq, using remote sensing techniques: they found that a 8.7% increase in urban areas and 25.8% decrease in green cover led to an average increment in the maximum LST by 3.79°C and 3.16°C in summer and winter,

* Corresponding author.
E-mail address: Faezeh.absalan@polymtl.ca (F. Absalan).

https://doi.org/10.1016/j.watres.2024.121490
Received 14 November 2023; Received in revised form 22 February 2024; Accepted 18 March 2024
Available online 28 March 2024

respectively. Smith et al. (2023) studied the effectiveness of albedo manipulation and urban greening on LST in seven cities in the United States. They found on average 0.18°C cooling per % albedo increase, 0.09°C cooling per % tree coverage, and 0.02°C cooling effect per % grass cover. Menberg et al. (2013) monitored groundwater temperature in shallow subsurface areas in six German cities and found 3-7°C regional differences between the urban and rural areas. In the province of Quebec, Canada like many other regions in the world, the climate trends are showing increased number of hot days (T>30°C) and an increase in the number and duration of heatwaves (Leveque et al., 2021). This will in turn increase the soil surface and subsurface temperature during summer. Since some of the city's infrastructure, notably the DWDS, is buried underground, creation of UHIs could potentially affect the drinking water temperature in the pipes.

Physical, chemical, and biological processes in the DWDS are greatly impacted by water temperature. Kimbrough (2019) studied the impact of the increasing air temperature on drinking water (supplied from surface waters) temperature and quality in four DWDS in Pasadena, United States, from 2001 to 2016. They found that a 1.6-°C increase in median nighttime temperature led to a 0.8 to 1.4-°C increase in median drinking water temperature, a significant decrease in disinfectant (chloramine) residual and a significant increase in nitrite concentrations (due to ammonia-oxidizing bacteria activity). Increased temperature also increases the rate of chlorine decay and disinfection by-products formation (Lai and Dzombak, 2021). While many countries such as Canada, United States, France, and UK monitor water temperature during their regulatory water quality monitoring programs, the Netherlands and Czech Republic have regulated drinking water temperature in the DWDS (Agudelo-Vera et al., 2020). Blokker and Pieterse-Quirijns (2013) used a micrometeorology model, and Agudelo-Vera et al. (2015) incorporated anthropogenic heat sources into the model, to predict soil temperature using meteorological information. Comparing the soil temperature modeling results with drinking water temperature measurements in a Dutch DWDS revealed that drinking water temperature at the average depth of 1 meter reaches its surrounding soil temperature. They reported that the drinking water temperature in several sampling points exceeded its regulatory threshold of 25°C in a relatively warm year. Considering the increasing trends in global air temperature, they expected this trend to be amplified in the future (Blokker and Pieterse-Quirijns, 2013).

While several studies have reported the impacts of UHI and green spaces on soil surface and subsurface temperature, their impact on drinking water temperature within the DWDS is not well understood. In a cold climate region such as Canada with water pipes buried at least 1.8 meters deep (to avoid freezing), it could be expected that the water temperature would not be impacted by the UHI effect. In this work, for the first time, we use a combined data-driven and model-driven approach to assess the impact of UHI and vegetation on drinking water temperature in a full scale DWDS. The case study is the city of Montreal (Quebec, Canada), with deeply buried pipes, and the study is carried out during summer (heatwaves) 2022. We continuously monitor water temperature in two full-scale sectors in Montreal DWDS – namely the 'vegetation-impacted zone' and the 'UHI-impacted zone'– for 2.5 months. The water temperatures in these two contrasting zones will be compared to investigate the impact of UHI on deeply buried pipes and will shed light on the effectiveness of city greening (vegetation increase) for moderating water temperature in DWDS during hot periods. It also evaluates the effectiveness of deeper pipe burial as a mitigative measure to solve the problem of water warming. Finally, we adapt and evaluate the water temperature model by Blokker and Pieterse-Quirijns (2013) to our case study.

2. Methodology

This study integrates both a data-driven (from field monitoring in a full-scale network) and a model-driven approach. Initially, water temperature in the DWDS was directly measured using temperature sensors (as described in section 2.2). Subsequently, a novel modeling approach (detailed in section 2.3), was employed to simulate water temperature throughout the network. Finally, the modeling results were compared with the direct measurements. The study consists of four main steps, namely: (i) the site selection for field data collection, (ii) temperature monitoring in the DWDS, (iii) soil temperature modeling, and (iv) drinking water temperature modeling including validation.

2.1. Study site selection for field data collection

For the temperature monitoring campaign, two study sites with contrasting land surface temperature and green coverage were selected. To select these two zones, the Landsat 8 images, classifying soil temperature into five distinct classes, were studied in combination with the green spaces map of Montreal using the QGIS 3.26.2 software. To ensure consistency in our results, we compared three Landsat 8 maps from the years 2013, 2016, and 2019, all with a resolution of 30m x 30m. Our objective was to confirm that there were no significant differences among these maps that could influence the choice of the study area (Donneesquebec, 2019). Finally, the 2019 map which was captured on June 9th, 2019, between 15:30 and 16:30 was selected (shown in Fig. 1. A). In this figure, the soil surface temperature is classified into five distinct classes. Class 1 is the cool islands, class 2 is the below average temperature zones, class 3 is the average temperature zones, class 4 is the above average zones, and class 5 is the heat islands. The zone on the left, the UHI-impacted zone, has a higher density of buildings and concrete/paved surfaces and a higher LST according to the Landsat image. The zone in the vicinity on the right, the vegetation-impacted zone, contains greener spaces such as parks, trees, bushes, and more shaded areas and has a lower LST. The two selected zones were connected to the same water treatment plant (WTP) which facilitates the water temperature comparison. Moreover, the two studied zones were close to one another to share the same meteorological conditions such as air temperature, wind speed, and direction.

2.2. Water temperature monitoring

With prior authorization from the City of Montreal, a comprehensive water temperature monitoring campaign was undertaken. This campaign involved door-to-door interactions with residents to request their permission to install temperature loggers in their building. This process which took several weeks and several visits to different parts of each sector resulted in the recruitment of 34 volunteers – 17 from each designated zone. In the UHI-impacted zone, 12 commercial buildings (restaurant, fire station, supermarket) and 5 residential buildings were monitored. In the vegetation-impacted zone, 10 residential buildings and 7 commercial buildings (supermarket, public pool, commercial center) were monitored. The next step was the installation of temperature loggers for water temperature measurement. The temperature loggers (EasyLog temperature probe data logger purchased in Montreal, Quebec with an accuracy of ±0.5°C), shown in Fig. 1.B, was installed on the service lines connecting the distribution pipes to each building. The visible part of the service lines was usually found in the basement, garage, or in some cases on the ground floor. The installation involved taping the copper element to the pipe exterior wall under insulation. A sample of one of the installations is shown in Fig. 1.C. Both the pipe material and the temperature probe material composed of copper, providing high conductivity and sufficiently accurate temperature measurement of the water within the pipes. The loggers measured and recorded temperature continuously every 5 minutes during the period of July to September 2022. This campaign resulted in an extensive database of the water temperature variations with more than 21,000 data points from each building. The placement of the monitoring points in the UHI-impacted zone and vegetation-impacted zone is displayed in Fig. 1. A, with the monitoring points marked with letters A to Q in each zone.

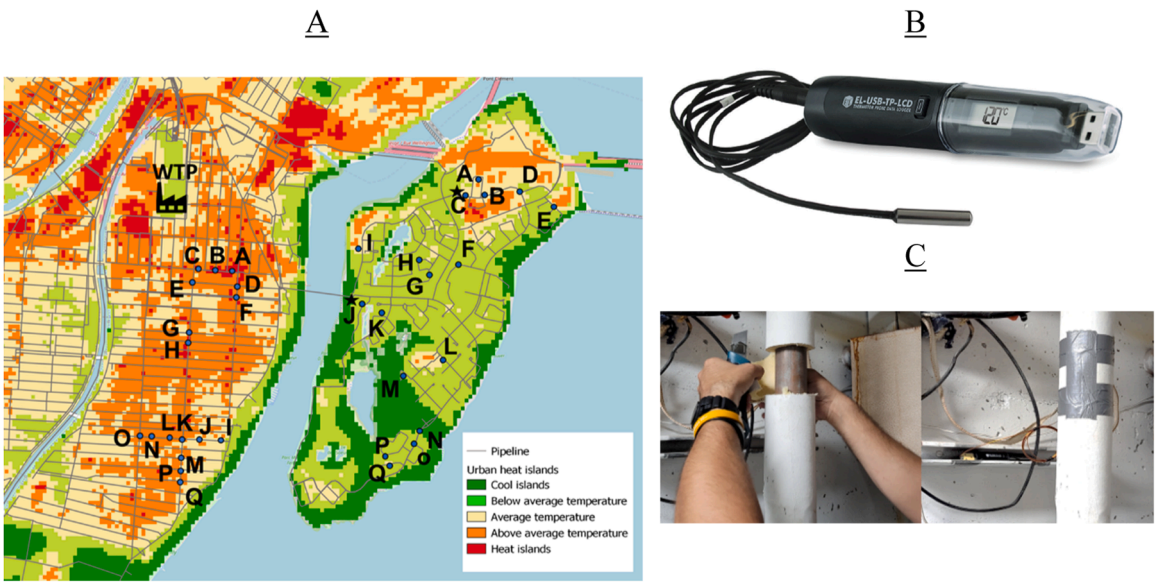

Fig. 1. A: Two monitoring zones – vegetation-impacted zone on the right and the UHI-impacted zone on the left, the WTP feeding both zones, and the placement of the temperature loggers indicated with letters, B: temperature probe data logger, and C: Installation of a temperature logger on the service line. Point C* is the north entrance and point J* is the east entrance connecting the UHI-impacted zone to the vegetation-impacted zone.

2.3. Modeling soil temperature

The soil temperature model by Blokker and Pieterse-Quirijns (2013) incorporating the data from the anthropogenic heat sources by Agudelo-Vera et al. (2017) is presented in Equation 1. This model requires meteorological data to model soil temperature. This type of information is publicly accessible, which makes the process more feasible both for researchers and utilities. Additionally, the model is capable of predicting soil temperature under various scenarios, taking into account diverse thermal and physical soil characteristics for each scenario. These scenarios encompass a spectrum from urban heat islands (warmest) to peri-urban areas (coolest). Given the five temperature classes derived from Landsat imagery in the chosen study zones (section 2.1), employing this model enables the modeling of local soil temperature values. This is achieved by associating each soil scenario with a specific zone on the map based on its Landsat surface temperature classification.

$$\rho_{soil} C_{p,\ soil} \frac{\partial T_{soil}}{\partial t} = \lambda_s \frac{\partial^2 T_{soil}}{\partial Z_s^2} + \frac{1}{\Delta z}\left(R_{net} + Q_F - \Delta Q_s - L_v E - \rho_{soil} C_{p,\ soil}(T_{SS} - T_{RL}) \,/\, R_g\right) \quad (1)$$

In this equation, ρ_{soil} (kg.m^{-3}) and $C_{p,\ soil}$ (J.kg^{-1}.K^{-1}) are the density and heat capacity of the soil. T_{soil} is the soil temperature, t is the time (h), z is the depth (m), and λ_s (W.m^{-1}.K^{-1}) is the thermal conductivity of the soil. R_{net} (W.m^{-2}) is the net radiation and Q_F (W.m^{-2}) represents the anthropogenic heat from the surface. T_{ss} is the soil surface temperature (K), T_{RL} is the roughness layer temperature (K), and R_g (W.m^{-2}) is the global radiation. ΔQ_s (W.m^{-2}) is the net surface and subsurface heat storage flux (uptake and release) which can also be written with Equation 2 (Agudelo-Vera et al., 2017). In this equation, a_1 (unitless), a_2 (W.m^{-2}), and a_3 (W.m^{-2}) are empirical coefficients for different surface types.

$$\Delta Q_s = a_1 R_{net} + a_2 \frac{\partial R_{net}}{\partial t} + a_3 \quad (2)$$

Equation 1 and Equation 2 were used to model soil temperature in five distinct soil scenarios corresponding to the five LST classes obtained from the satellite images. The average soil density (2710 kg.m^{-3}), specific heat capacity (10^3 J.kg^{-1}.K^{-1}), and heat conductivity (1.6 W.m^{-1}.K^{-1} for class 1 to 4) were taken from a local study conducted by Tarnawski et al. (2015) on average thermal properties of soils in Montreal. The heat conductivity for class 5 or the heat islands was set to 2.6 W.m^{-1}.K^{-1} based on the study of Agudelo-Vera et al. (2017). The specific coefficients corresponding to each of the five soil coverage classifications (local climate zones) are based on a study conducted by Stewart and Oke (2012) and presented in Table 1.S in the supplementary material. The average albedo of Montreal (0.19) was also taken from a study conducted by Frie et al. (2022) reporting the average albedo of Montreal. Albedo is a measure of surface reflectivity which quantifies what fraction of solar radiation is reflected and not absorbed by the soil (Frie et al., 2022). Hourly meteorological data of air temperature (°C), wind speed (m/s), Wind direction (degree), solar radiation (J/cm^2), and Precipitation (mm) from the McTavish weather station in Montreal was obtained from the Environment and Climate Change Department of the Government of Canada. The duration of the data was from 2016 to 2022 and the selected weather station was the closest to the study sites. The data was then incorporated in the soil temperature model via MATLAB R 2021b and soil temperature was predicted at different depths underground for all the five scenarios (Agudelo-Vera et al., 2017).

2.4. Modeling and validating water temperature

The water temperature model is presented in Equation 3, Equation 4, and Equation 5 (Blokker and Pieterse-Quirijns, 2013).

$$\frac{dT_{water}}{dt} = k\ (T_{outer\ wall} - T_{water}) \quad (3)$$

$$k = \frac{4.\alpha_{water}}{D_1^2\left(\frac{1}{Nu} + \frac{\lambda_{water}.ln\left(\frac{D_2}{D_1}\right)}{2.\lambda_{pipe}}\right)} \quad (4)$$

$$D_2 = D_1 + 2.\ pipewall\_ratio.D_1 \quad (5)$$

$T_{outer\ wall}$ is the soil temperatures surrounding the pipe which is used as the pipe boundary condition. α_{water} is the thermal conductivity of water (1.36e^{-7} m^2.S^{-1}) and λ_{water} is the specific conductivity of water (0.57 W.m^{-1}.K^{-1}). λ_{pipe} is 15 W.m^{-1}.K^{-1} for stainless steel, 60 W.m^{-1}.K^{-1} for cast iron, 0.43 W.m^{-1}.K^{-1} for asbestos cement, and 0.16 W.m^{-1}.

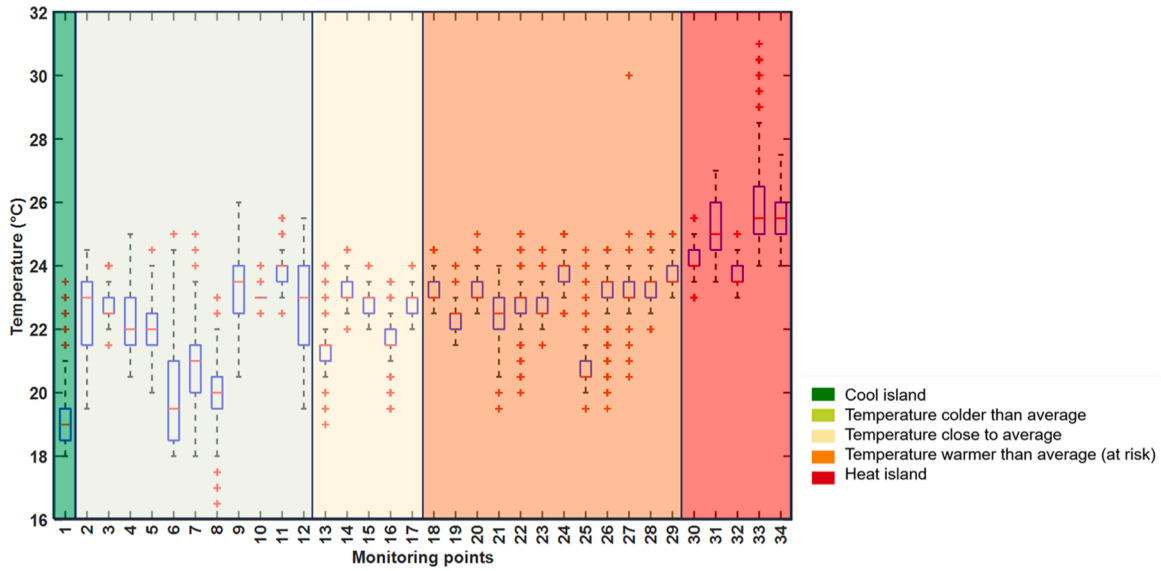

Fig. 2. Monitoring results in the 34 sampling points in UHI-impacted zone and vegetation-impacted zone during the period of July 27th to August 12th. The boxes present, 25th percentile, median, and 75th percentile. The whiskers present the minimum and maximum and the outliers are presented with red plus signs.

K^{-1} for PVC pipes. *Nu* is the Nusselt number equal to $0.03.Pr^{0.33}.Re^{0.8}$ assuming turbulent flow. D_1 is the pipe inside diameter (mm), and D_2 is the outer pipe diameter (mm) with the assumption of pipewall ratio equal to 0.07. The boundary condition for the underground pipes – used as the pipe outer wall temperature in the model – was determined by using the resulting soil temperature at a depth of 1.8 m from the previous step. The soil temperature variations were studied for 24 hours each day to see whether we can use one single soil temperature for the whole day in the equation. After verifying that the soil temperature variation was 0.5°C on average, one single soil temperature – the soil temperature at midday – was used as the $T_{outer\ wall}$ and integrated into Equation 3.

Overlaying the LST maps from Landsat imagery from step 1 onto the hydraulic model of the city helped categorizing pipes into five distinct temperature classes. Subsequently, based on the temperature classification, a distinct pipe wall temperature was assigned to $T_{outer\ wall}$ in the soil temperature model, allowing the accurate prediction of water temperature variations within every single pipe based on the local soil temperature surrounding each pipe. The hydraulic network of the city was modeled using WaterGEMS (10.04.00.108). The water temperature modeling was carried out with the Multi-Species Analysis, based on the EPANET-MSX model with WaterGEMS user interface.

Due to the absence of water meters in buildings, specific water demand per household couldn't be measured. To address this limitation, the average daily water demand pattern in the city of Montreal in summer (Figure 1.S in the supplementary material) was applied to the hydraulic model. A 7-day water quality simulation ensued to allow for system-wide stabilization. Each day involved a new soil temperature ($T_{outer\ wall}$) in the model, and the stabilized water temperature variations were compared to field measurements. Model validation employed statistical tests in MATLAB R2021b. Additionally, a water age simulation was conducted for all 34 monitored points using a 14-day simulation period with a hydraulic timestep of 1 hour. The outcome includes the hourly variations in water age at each node.

3. Results

3.1. Temperature monitoring results

After recovering all the temperature loggers, the temperature data were extracted for analysis. Fig. 2 shows the correlation between monitored temperatures and the LST classifications based on satellite image. Each boxplot present the continuous (every 5 minutes) water temperatures in one monitoring point during the period of July 27th to August 12th, resulting in 34 box plots. It is worth noting that one participant withdrew from the study after August 12th. To ensure a fair and uniform comparison among all monitoring points, we limited the data presentation on this figure to this period. Table 1 presents the average values for minimum, median, and maximum water temperatures for each LST classification. A distinct warming trend is observed as soil temperature classifications increase from 1 to 5. The median recorded temperature difference between class 1 and class 5 reaches a maximum of 6.5°C, with an average difference of 5.7°C, indicating a significant warming effect on water temperatures when transitioning from low LST zones to high LST zones. Notably, classes 3 and 4 exhibit minimal temperature differences, primarily due to their proximity, where water passes through class 4 soils (warmer areas) to reach class 3 soils. In contrast, Class 5, the heat islands, shows temperatures 1.6-1.8°C higher in minimum and median, and 2.8°C higher in maximum compared to class 4.

Fig. 3 illustrates the water temperature monitoring results plotted against the average daily water age at each monitoring point. Our findings reveal no discernible increase in water temperature with an increase in water age at each monitored point. Previous studies by Agudelo-Vera et al. (2020) on a Dutch DWDS suggested that longer water residence times (greater than 12 hours) in the network led to

Table 1
The minimum, median, and maximum recorded temperatures from the temperature loggers with regards to their LST classification based on the satellite image.

LST classification based on Landsat image		Class 1	Class 2	Class 3	Class 4	Class 5
Monitored water temperature (°C)	Average minimum (°C)	18	20.18	21.6	22.04	23.6
	Average median (°C)	19	22.11	22.4	22.88	24.7
	Average maximum (°C)	21	24.18	23.1	23.71	26.5

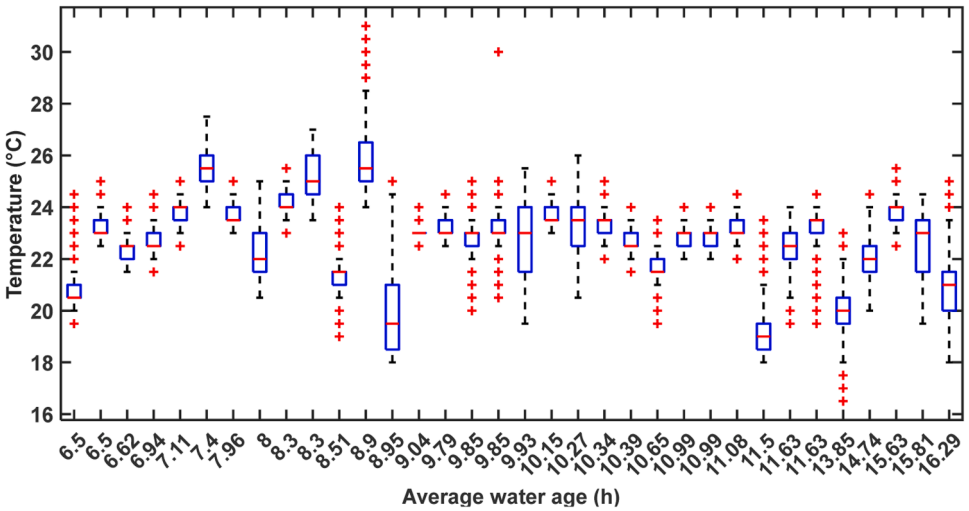

Fig. 3. Measured water temperatures vs. average water age at each monitored point between July 27th and August 12th. The boxes present the 25th percentile, median, and 75th percentile. The whiskers present the minimum and maximum temperatures, and the outliers are presented with red plus signs.

elevated temperatures. They also noted a trend of increasing temperatures further downstream from the WTP. Similarly, Machell and Boxall (2014) conducted a study in the UK, investigating the relationship between measured water temperatures and water age. Their findings showed a rising trend in temperature for samples taken from pipes with longer water ages. It is important to note that in both previous cases, the source water temperature was considerably lower than the surrounding soil temperature. For example, in the Dutch case study (Blokker and Pieterse-Quirijns, 2013), the source water originated from underground sources with an average temperature of 10°C, while a constant soil temperature of 25°C was considered for modeling water temperature in the DWDS. As a result, longer contact time (water age) of water in warmer soil leads to an increased water temperature. In contrast, our studied city utilizes surface water from a river, which exhibits higher temperatures during the summer (ranging from 22-25°C). In this scenario, the water temperature can be influenced by various soil coverages and, consequently, different soil temperatures along its journey to the customer's building. This can either lead to a cooling or heating effect based on the surrounding soil temperature.

To study the correlation between water temperature and air temperatures, Fig. 4.A shows the average hourly monitored water temperatures along with the hourly air temperature plotted together for the period of July 27th to September 1st. In the UHI-impacted zone, the average hourly water temperature fluctuated between 19.9°C and 30.9°C, with an average temperature of 23.7°C over the entire period. In contrast, the vegetation-impacted zone exhibited water temperatures between 16.6°C and 26°C, with an average temperature of 22.3°C throughout the same period. The recorded air temperatures ranged from a minimum of 12.3°C on September 1st to a maximum of 31.6°C on August 6th. Comparing the peak dates for water temperature (e.g., August 10th, 16th, 25th, 30th) with the peak dates for air temperature (e.g., August 6th, 7th, 20th, and 29th) does not confirm any immediate influence of air temperature on water temperature. To investigate the potential correlation between hourly air temperatures and water temperatures in all monitoring points, we calculated the correlation coefficient (r) and the coefficient of determination (R^2) between air and water temperatures. In the UHI-impacted zone, r values ranged from -0.44 to 0.6 across monitored points, with an average r of 0.07. Conversely, in the vegetation-impacted zone, r values fell within the range of -0.4 to 0.31 across monitored points, with an average r of -0.05.

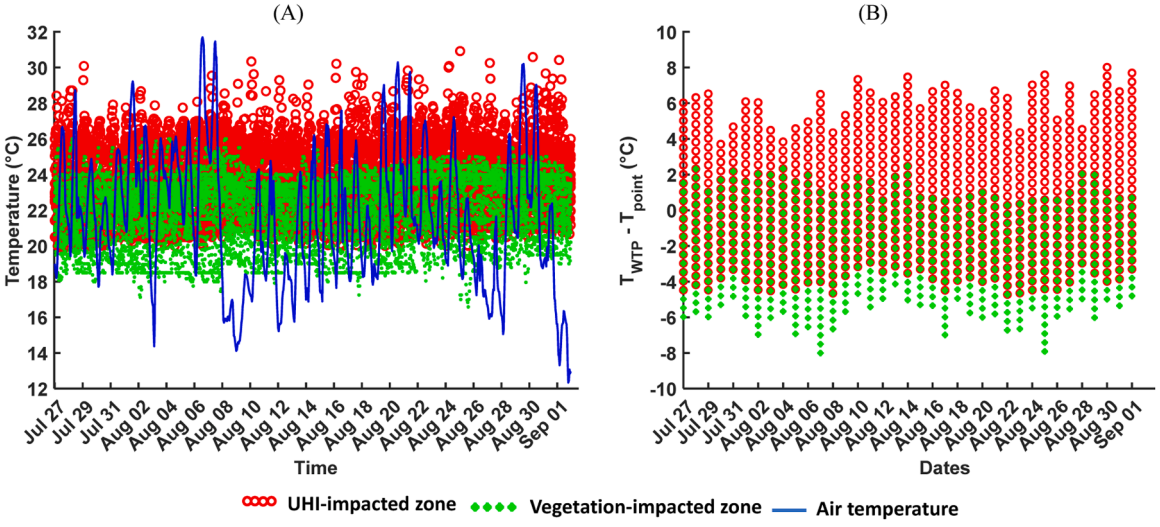

Fig. 4. A: Average hourly temperatures in all 34 monitored points and the average hourly air temperature during the period of July 27th to September 1st, B: temperature differences between the WTP average daily temperature (T_{WTP}) and the recorded hourly temperatures at each location (T_{point}) during the period of July 27th to September 1st.

The results suggest that no definitive correlation exists between hourly air and water within the DWDS. In the vegetation-impacted zone, R^2 values ranged between 0 and 0.15 across monitored points with an average of 0.02. In the UHI-impacted zone, R^2 values ranged between 0 and 0.36 across all the points with an average of 0.07. The results of R^2 indicate a relatively low overall fit between the variables. This suggests that the variability in water temperature is not well explained by the variability in air temperature.

To estimate the cooling or warming effects in each zone, we calculated the difference between the hourly temperatures at each point and the temperature at WTP exit for the period of August 27th to September 1st. The results are presented in Fig. 4.B. Our findings reveal that in the UHI-impacted zone, the maximum warming observed was 8°C on August 25th, while in the vegetation-impacted zone, the maximum warming reached 2.5°C on August 14th. In the vegetation-impacted zone, the maximum cooling was 8°C on August 7th and August 25th and the maximum cooling in the UHI-impacted zone was 4.7°C on August 9th. On average, the cooling effect in the vegetation-impacted zone was 1.6°C, while the UHI-impacted zone showed an average cooling of 0.2°C across all monitored points. It's worth noting that water is transferred to the vegetation-impacted zone via two connecting pipes that pass under the river. The northern connecting pipe is a 20-inch diameter with a water travel time of 1.7 hours, while the eastern connecting pipe is 30 inches in diameter with the same travel time. In the northern region, the hourly average temperature difference between the WTP and point C, the north entrance, in the vegetation-impacted zone ranged from 0 to 2.5°C, with an average of 1.4°C throughout the study period. In the east, the hourly average temperature difference between point F in the UHI-impacted zone and point J, the east entrance, in the vegetation-impacted zone varied from -0.5°C to 3°C, averaging 1.5°C. A plot showing the monitored temperatures in the vegetation-impacted zone with regards to the two entrance temperatures is provided in Figure 2.S in the supplementary material. Comparing the monitored temperatures at the two entrance points with the rest of the points showed that the two entrance nodes can be considered the warmest points in the vegetation-impacted zone, while the rest of the monitored points generally exhibit lower temperatures. This indicates that the cooling effect in the vegetation-impacted zone is influenced not only by the river but also by the passage of water through the zone, which has a lower soil temperature.

3.2. Soil temperature modeling results

Fig. 5 shows the hourly soil temperature modeling results at the depth of 1.8 m across five soil scenarios between July 27th and August 12th. During this period, the average soil temperature for class 1 was 18.5°C. Moving from class 1 to 5, the average soil temperatures increased by 6.2°C. As previously shown in Fig. 2, the maximum difference between median water temperature measurements for class 1 and 5 is 6.5°C, which aligns closely with the difference between the average modeled soil temperatures between these two classes. Fig. 5 also contains the minimum, average, and maximum daily water temperatures from the monitoring campaign during the same period to show the alignment between modeled soil temperatures and measured water temperatures. According to Fig. 5, the maximum daily water temperatures do not exceed the values associated with class 5 soil temperature, except in three locations within the UHI-impacted zone, where the maximum water temperature reached up to 30.9°C but the maximum soil temperature did not exceed 26°C. On the other hand, the minimum daily water temperatures do not fall below the minimum soil temperatures, except at two points within the vegetation-impacted zone, where the minimum daily water temperature reached down to 16.6°C, whereas soil temperature did not go below 18°C.

To investigate the effect of deeper pipe burial on soil temperature, the modeled soil temperature at two different depth of 1 m (as in the Dutch case study by Blokker and Pieterse-Quirijns (2013)) and 1.8 meter used in the Canadian DWDS were compared. At 1 m depth, the soil is on average 3.98°C cooler than the surface and at 1.8 m depth, the soil is on average 6.91°C cooler than the surface. So, increasing the burial depth from 1 m to 1.8 m in the studied area leads to a 2.9°C cooling effect on average soil temperature surrounding pipes. This value could vary in each case study based on the local soil conductive properties.

3.3. Water temperature modeling results

The water temperature modeling results during the period of August 1st to August 12th are presented in Fig. 6 along with the soil temperature modeling results and water temperature measurements. As seen in the figure, the variations in the measured water temperature are much greater than the modeled water temperature variations. These variations are due to different water consumption habits (time, duration, and

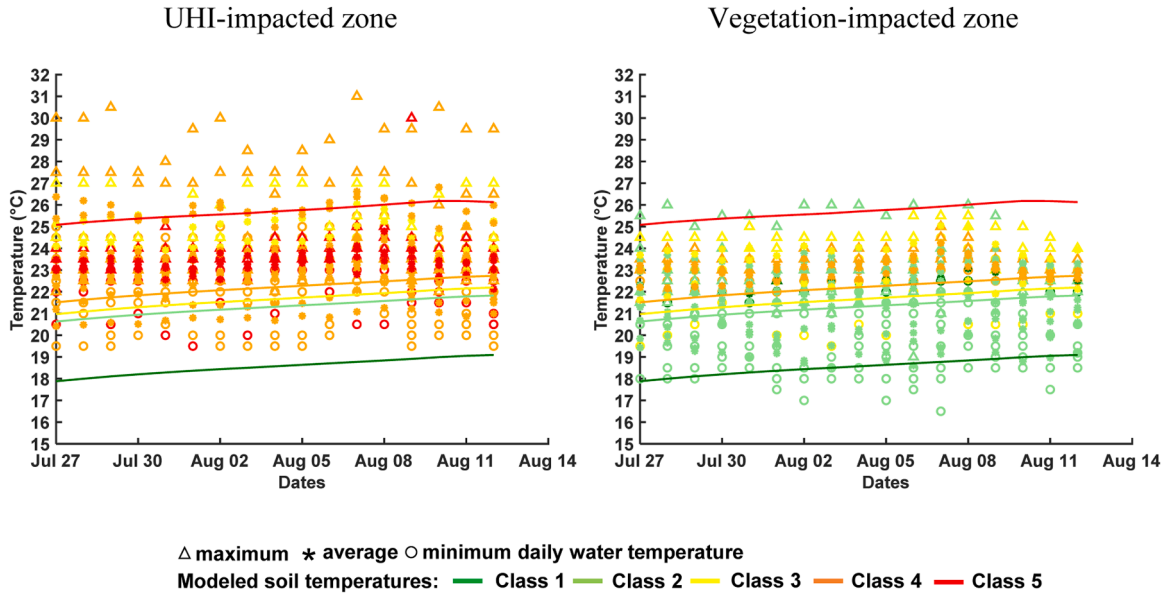

Fig. 5. Modeled soil temperatures in five classes plotted along the minimum, average, and maximum daily measured water temperatures in all the 17 monitoring points from July 27th to August 12th. The water temperature records from each point is color-coded based on the placement of each point with regards to the soil classification.

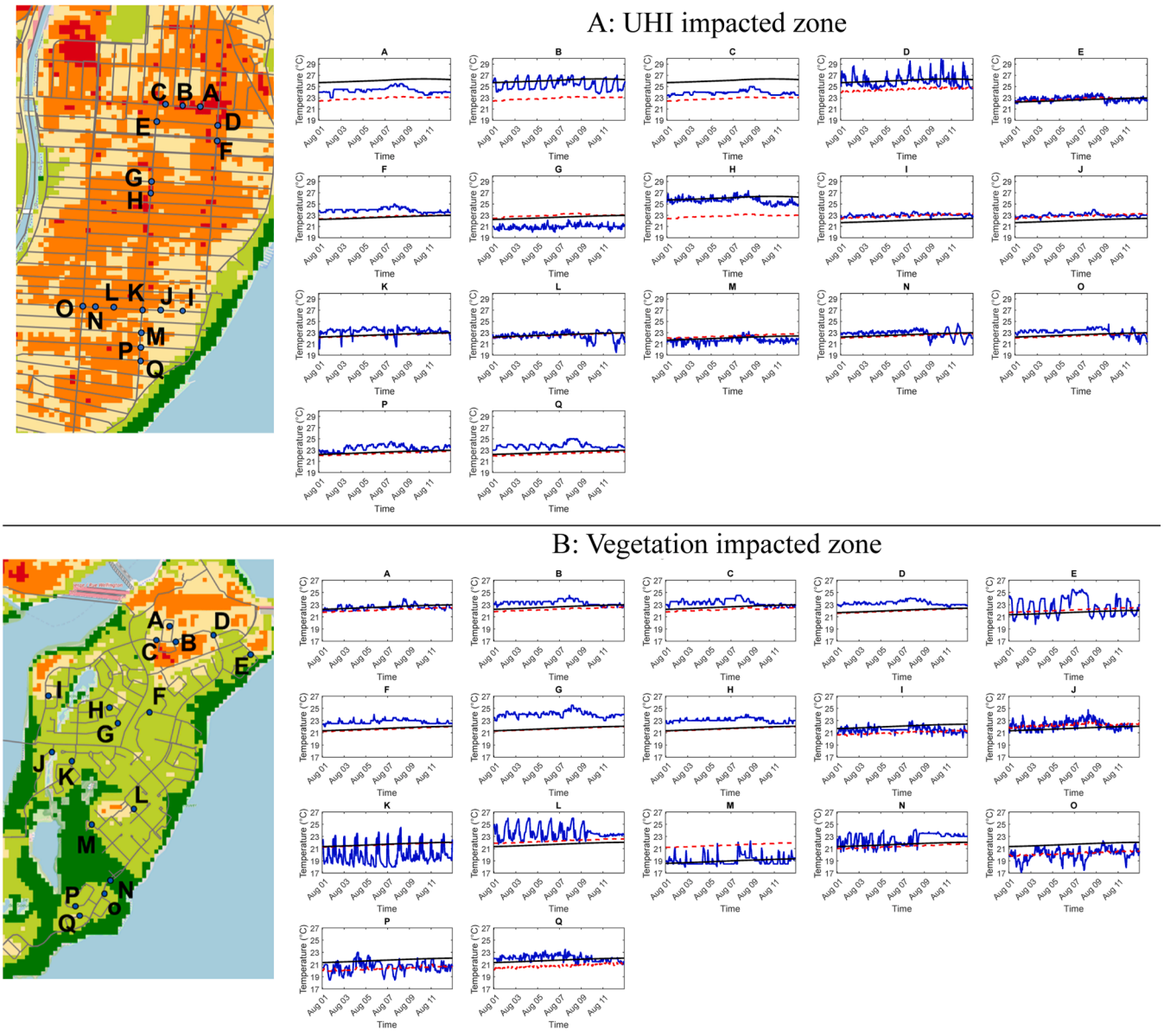

Fig. 6. Water temperature modeling and monitoring results and soil temperature modeling results in all the 17 monitored points in the UHI-impacted zone (6A) and vegetation-impacted zones (6B) between August 1st and 12th. Each figure corresponds to one monitoring point in the network with their corresponding location indicated on the map with letters. Legend:— measured water temperature, — modeled water temperature,— modeled local soil temperature.

intensity of using bathroom, shower, cooking, garden watering, etc.), type of building (residential, non-residential), and the number of residents present in each building. For example, in the vegetation-impacted zone, the participants in points L and N were on vacation during August 9th to 12th and the participants in point I were on vacation from August 5th to 8th. As shown in Fig. 6, the water temperature stabilizes in these points during these periods, reflecting water stagnation in the service lines during these periods. Due to the absence of specific demand information for each household and the utilization of a similar demand pattern in WaterGEMS corresponding to the daily average demand pattern in the city for August, it was not possible to compare the hourly results. Therefore, the daily average modeled and measured temperatures were compared to assess the quality of prediction.

It's important to emphasize that the soil temperature data in Fig. 6 pertains to the local soil temperature in the immediate vicinity of each monitoring point. In contrast, water temperature modeling reflects the composite influence of upstream conditions, as the water passes through various pipes. Each of these pipes has different soil temperatures, affecting the outer wall temperature ($T_{outer\ wall}$) and thereby impacting the overall water temperature. In Fig. 6.A for the UHI-impacted zone, although points A, B, C, D, and H are situated in soil class 5, the modeled water temperature in these locations is lower than the modeled soil temperature. This discrepancy arises from the fact that the pipes connected to these points originate from areas with lower soil temperature classes 4 and 3. The modeled water temperature reflects the entire journey of water within the DWDS, hence appearing lower than the local soil temperature. In the rest of the points, where the local soil temperature aligns more closely with the average pipe temperature that water flows through, the soil/water temperature difference is minimized. Similarly, in Fig. 6.B for the vegetation-impacted zone, water arriving from the warmer UHI-impacted zone initially maintains a higher temperature at points F, G, and H, remaining under the influence of the upstream soil temperature. However, as it traverses through cooler pipes within the vegetation-impacted zone, the soil/water temperature differential declines. Subsequently, at point M, where the water passes through class 3 pipes, the modeled water temperature surpasses the local

soil temperature.

To illustrate the impact of soil temperature on modeled water temperatures, the water temperature variations from August 1st to 12th are plotted in Fig. 7 with boxplots in an ascending order based on the average water age of each point in the DWDS. The point codes are specified under each boxplot and the average water travel time at each point is specified above each boxplot. Fig. 7.A shows the results in the UHI-impacted zone. Some points were in the vicinity of one another and had similar water travel times, so only the points with different water travel times are reported. Points M and J, belonging to LST class 3 with an average modeled soil temperature of 21.8°C, exhibit water temperatures higher than their respective local soil temperatures. These two class-3 points are in proximity to class 4 soils, with an average temperature of 22.4°C, and water sourced from class 4 soils with higher average temperatures reaches them. This underscores the influence of upstream soil temperature on water temperature, highlighting that soil temperature affects water temperature not only at the pipe location but also during the water trajectory. Fig. 7.B presents results for the vegetation-impacted zone. Given the presence of two entrances and water mixing, we focused on water sourced exclusively from the east entrance (or point J in the vegetation-impacted zone). A trace analysis in WaterGEMS determined the percentage of water sourced from the north and east entrances, enabling us to isolate nodes receiving 100% of their supply from the east entrance. All the points in the plot belong to soil class 2, with an average soil temperature of 21.5°C. It is evident that lower soil temperature results in lower water temperature, aligning with the model's predictions. Furthermore, increased water travel time within the vegetation-impacted zone leads to decreased modeled water temperatures, highlighting the impact of soil temperature on water temperature variations and the coherence between soil and water temperature models. Notably, points Q and P are located near soil class 1, and the pipes serving them pass through cooler soils with an average temperature of 18.7°C.

The goodness of prediction statistics between measured and predicted daily water temperatures is presented in Table 2. This table contains the minimum/average/maximum prediction error for each point, the root means square error (*RMSE*) for the actual values, the *RMSE* for the normalized values, and the *P-value*. In the UHI-impacted zone, the minimum prediction error is between 0°C and 1.98°C, the average prediction error is between 0.2°C and 2.78°C, and the maximum prediction error is between 0.33°C and 3.26°C across all 17 points. In the vegetation impacted zone, the minimum prediction error is between 0.01°C and 1.66°C, the average prediction error is between 0.32°C and 2.53°C, and the maximum prediction error is between 0.75°C and 3.19°C across all 17 points. In the vegetation impacted zone, the *RMSE* ranges between 0.39°C and 2.55°C and, the normalized *RMSE* ranges between 0.2 and 0.54, and the average *P-value* is 2.6E-03. In the UHI impacted zone, the *RMSE* ranges between 0.23°C and 2.82°C, the normalized *RMSE* ranges between 0.24 and 0.52, and the average P-value is 6.12E-04. Normalized *RMSE* ranges between 0 and 1 and a normalized *RMSE* below 0.5 could be indicative of a reasonably good fit. Additionally, to examine the correlation between the predicted and measured temperature timeseries and the temporal alignment of the predicted results with the measured data, a cross correlation analysis was performed, and the results are presented in Figure 3.S in supplementary materials. A cross-correlation equal to 1 at lag 0 at all points suggests that the predictive model is performing well for all points, replicating the variations and trends in the measured temperature time series. These statistics show the significance of the model prediction.

4. Discussion

The drinking water temperature monitoring results showed that water at 1.8 m underground pipes can still be under the influence of heatwaves and UHIs during summer. The modeling results showed that the average soil temperature at 1.8 m depth is on average 2.93°C cooler than the soil temperature at 1 m, suggesting that pipe burial could be an effective measure for dampening the water warming effect during hot periods. However, in our case, deeper pipe burial did not eradicate the issue of water warming and the water temperature in the studied network would still go as high as 32°C (hourly average of 30.9°C) during summer days.

Our hypothesis suggests that service lines reflect DWDS water temperature during high-demand hours. During low-demand and stagnation periods, service line temperature may vary from DWDS, influenced by surrounding soil temperature. In UHI-impacted zones, prolonged stagnation could elevate temperatures due to extended contact with the warm environment, while in vegetation-impacted areas, temperatures might decrease due to prolonged contact with the cooler environment. The lack of water meters and information about stagnation periods in buildings prevented verification of this hypothesis. Nevertheless, stagnation occurred in both zones, but significantly elevated temperatures were only observed in the UHI-impacted zone. Consequently, whether stagnation occurred or not, the UHI-impacted zone consistently exhibited higher temperature readings.

Comparing the heating and cooling effect in the two contrasting zones showed that the maximum heating effect in the UHI-impacted zone was 5.5°C higher than the maximum heating in the vegetation-impacted zone. Moreover, the maximum cooling effect in the vegetation impacted zone was 3.3°C higher than the maximum cooling in the

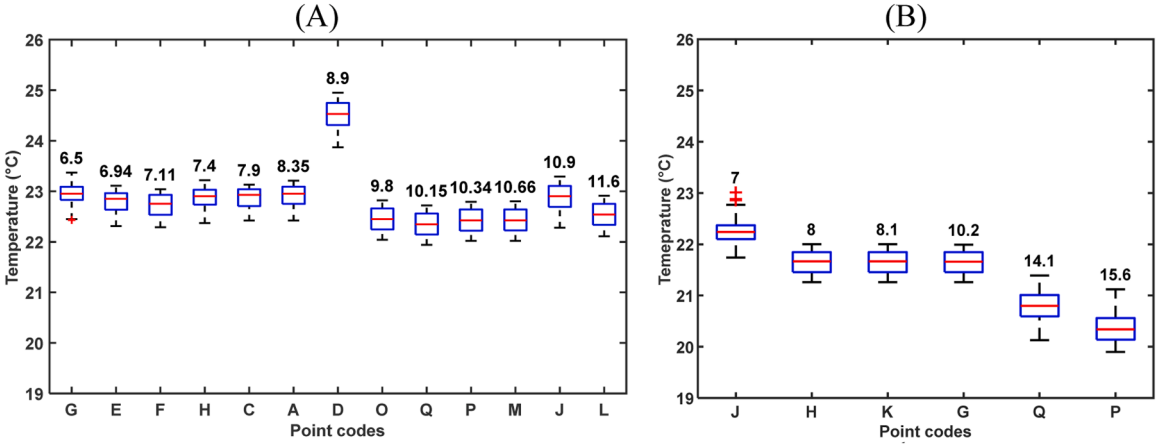

Fig. 7. Modeled water temperatures during water travel time from August 1st to 12th in A: the UHI-impacted zone and B: vegetation-impacted zone from east entrance exclusively. The boxes present, 25th percentile, median, and 75th percentile. The whiskers present the minimum and maximum and the outliers are presented with red plus signs.

Table 2
Goodness of prediction statistics in the UHI-impacted and vegetation-impacted zones (period: August 1st to August 12th).

		A	B	C	D	E	F	G	H	I	J	K	L	M	N	O	P	Q
Vegetation-impacted zone	Minimum Error (°C)	0.17	0.28	0.31	0.56	0.01	0.64	1.53	0.58	0.24	0.10	1.06	0.57	1.66	0.51	0.07	0.05	0.53
	Average Error (°C)	0.45	1.11	1.19	1.33	0.75	1.25	2.42	1.45	0.55	0.34	1.75	1.38	2.52	1.24	0.42	0.34	1.36
	Maximum Error (°C)	0.76	1.62	1.93	1.83	2.87	1.55	3.19	1.82	0.82	0.75	2.57	1.91	3.04	1.98	1.09	1.34	1.81
	RMSE (°C)	0.48	1.18	1.27	1.38	1.14	1.28	2.45	1.49	0.59	0.39	1.81	1.43	2.55	1.33	0.53	0.53	1.43
	Normalized *RMSE*	0.20	0.44	0.44	0.44	0.45	0.38	0.41	0.40	0.39	0.30	0.39	0.47	0.38	0.26	0.28	0.37	0.54
	P-Value	8.33E-06	4.11E-06	7.61E-06	4.68E-07	2.06E-02	3.35E-08	5.16E-09	1.11E-07	4.85E-06	2.39E-04	3.83E-07	4.05E-07	3.06E-09	6.57E-06	2.00E-03	2.14E-02	1.99E-06
UHI-impacted zone	Minimum Error (°C)	0.74	1.68	0.64	0.62	0.10	0.47	1.67	1.98	0.00	0.12	0.14	0.03	0.11	0.01	0.01	0.46	0.70
	Average Error (°C)	1.41	2.42	1.05	1.47	0.26	1.14	2.02	2.78	0.20	0.27	0.73	0.35	0.78	0.64	0.80	0.95	1.42
	Maximum Error (°C)	2.06	2.95	1.52	2.04	0.41	1.65	2.18	3.26	0.33	0.41	1.21	1.39	1.17	0.91	1.26	1.51	2.33
	RMSE	1.46	2.45	1.08	1.54	0.27	1.21	2.02	2.82	0.23	0.28	0.80	0.51	0.84	0.69	0.90	1.02	1.48
	Normalized *RMSE*	0.41	0.36	0.40	0.34	0.46	0.48	0.24	0.39	0.32	0.42	0.43	0.48	0.40	0.52	0.50	0.34	0.47
	P-Value	1.09E-07	1.23E-10	3.32E-08	1.88E-07	1.12E-06	1.13E-06	2.93E-14	4.62E-10	1.52E-04	9.88E-08	1.70E-05	1.02E-02	3.03E-06	6.21E-06	4.48E-05	3.49E-06	2.61E-07

UHI-impacted zone (Fig. 4.B). The influence of local climate zones on drinking water temperature hasn't been explored in prior studies. Our findings align with existing research, indicating increased LST in urban areas with impervious surfaces and lower LST in green spaces with parks and shadows (Alexander, 2021; Edan et al., 2021; Kafy et al., 2022; Smith et al., 2023; Zhu et al., 2021).

The peak air temperatures did not coincide with peak water temperatures. The alignment between measured water temperatures and soil temperature modeling results indicates that the temperature of drinking water in pipelines is more influenced by the surrounding soil environment than air temperature. Soil temperature is a result of the preceding air temperature and other weather conditions, but there is no linear correlation. This aligns with the findings of Blokker and Pieterse-Quirijns (2013), who demonstrated that drinking water temperature in DWDS reflects the surrounding soil temperature.

Throughout the study, raw water temperature at the WTP inlet ranged from 21°C to 24°C, and treated water temperature varied between 23°C and 25°C. There was no discernible relationship between source water temperature and drinking water temperature at monitoring points. This is consistent with the observations of Agudelo-Vera et al. (2015), who found no correlation between source water temperature and tap water temperature in Dutch distribution networks, affirming the influence of surrounding soil temperature on water temperature.

Studying monitored water temperature variations with regards to average daily water age within the DWDS showed no correlation, suggesting that the soil subsurface temperature during the water travel time and the contact time between water and each specific soil (or pipe wall) temperature is more important than the overall time the water has spent in the network.

The observed disparities in water temperature in this study could potentially have implications for water quality management practices in the DWDS. Firstly, in chlorinated networks such as this case study, it is commonly reported that the extremities of the network are more prone to microbial risks due to longer water travel times and therefore, depletion of chlorine. As a result, network extremities are chosen for regulatory water quality monitoring or for adjusting the applied chlorine dosage at the WTP to ensure sufficient chlorine coverage across network. The present work showed that the points in the UHI-impacted zone with a lower residence time exhibited the highest recorded temperatures up to 32°C, which could potentially lead to higher rates of chlorine decay and lower residual chlorine in these zones. Secondly, the hotspots in the networks are not considered in the choice of sampling points for regulatory monitoring. These hot zones could be prone to insufficient chlorine residual or elevated disinfection by-product levels. This matter requires further investigation to assess the potential risks of hot zones on chemical and microbial drinking water quality in DWDS. Finally, the potential risks of such extreme temperatures for pathogen regrowth within the DWDS requires more attention. For example, *Legionella pneumophila* (*Lp*), an opportunistic pathogens responsible for the potentially fatal Legionnaire's disease, is monitored mainly in cooling towers and buildings, assuming minimal *Lp* growth in the DWDS, largely associating it with water stagnation and heating within buildings (National Academies of Sciences, 2019). Although there are no specific regulations for *Lp* in the DS, the "Guidelines on Drinking Water Distribution Systems Best Practices" for Quebec municipalities (Quebec Government, 2023) suggests maintaining a minimum free chlorine of 0.1 mg/L in the DWDS to prevent microbial regrowth. Chlorine monitoring sites are typically situated at the peripheries and dead-end points. Consequently, the impact of the UHIs within the city on chlorine levels remains unexplored, and the potential effects of temperature variations on *Lp* growth in the DWDS are not taken into account.

The results of this study were a proof of the effectiveness of greening as a solution to dampen the extreme heatwaves and UHI effect on DWDS, during summer, and can reduce the level of exposure of urban communities to heat. Examining water temperature variations along the water path in DWDS (Fig. 7) highlighted the impact of the water trajectory on local water temperature and the importance of soil temperatures surrounding the pipes, i.e., beyond local soil temperature alone. To ensure effectiveness, greening should be applied over a certain pipe length, including upstream from warmer soils, rather than focusing solely on individual pipes. This interplay between soil temperature, water trajectory, and local water temperature provides valuable insights into the dynamics of the water temperature in the DWDS. To evaluate the effectiveness of greening in moderating water temperature, the proposed modeling approach offers great potential.

The proposed approach for water temperature modeling combined with satellite imagery across diverse types of soil coverage holds great potential to enhance strategic greening initiatives and supplement decision-making processes. Furthermore, our approach can aid in the optimal placement of water quality sensors within DWDS, considering hot zones impact. In the context of climate change adaptation, addressing disparities in drinking water temperature within cities becomes imperative. Investigating the implications of the observed disparities for water quality and public health is a critical next step.

Discrepancies between modeled and measured water temperatures stem from limitations and uncertainties in the modeling and monitoring process. The soil temperature model lacks calibration with field measurements. Relying on an average soil conductivity value for the Montreal Island from Tarnawski et al. (2015) may not accurately represent local conditions considering variations in pipe fillings, soil coverage, and heat conductivities. The parameter 'Q_f' in the soil temperature

model, representing anthropogenic heat sources, is adapted from Stewart and Oke (2012) study for different urban settings. Achieving a more realistic prediction requires detailed knowledge of underground heat sources like subway tunnels, geothermal systems, district heating systems, power plants, landfills, and buildings, as well as local thermal and hydraulic properties of soils in each zone (Kreitmair et al., 2020; Menberg et al., 2013). For instance, in UHI-impacted zones, where water temperatures exceeded the maximum soil temperature (points D and F), proximity to a subway station emitting excess heat from tunnels was observed. In the absence of such extensive data and resources, remote sensing techniques using LST maps offer a viable alternative. The limitation in the water temperature modeling process stems from the absence of specific demand patterns for individual buildings. This leads to the application of a uniform consumption pattern to all network nodes, which fails to accurately capture real variations in consumption. In terms of limitations in temperature monitoring, directly measuring water temperature inside the pipes was impractical due to the extended monitoring period (2.5 months) and the continuous nature of the monitoring process. Implementing such direct measurement could disrupt the normal operating conditions of the network. Consequently, temperature sensors were attached to the exterior of the service lines connecting the DWDS to each building. Because this condition applied uniformly to all monitored points, it is assumed that any bias introduced was consistent across all points, allowing for a valid comparison of water temperatures among different buildings. Moreover, unforeseen factors during the monitoring period, such as unknown vacation periods, flushing/firefighting water demand, connections to temporary networks, or routine maintenance activities, could have influenced both the water trajectory and demand, thereby affecting the drinking water temperature. These factors were not considered in the water temperature model.

5. Conclusion

The study's outcomes reveal key insights into the impact of heat islands and vegetation on drinking water temperature:

- Even in cold climates, deeply buried pipes at 1.8 m can be susceptible to the influence of heat islands during summer. In areas characterized by extensive UHI impact and limited vegetation, an important warming of up to 8°C was observed from the WTP to the service lines connected to consumer buildings. Conversely, zones with higher vegetation cover exhibited remarkable cooling, of up to 8°C.
- Soil temperature was found to be a superior indicator of water temperature variations compared to the local air temperature. This finding supports the utility of such modeling tool to improve water management in cities.
- Prolonged water residence times in the DWDS did not lead to higher water temperatures. This can be attributed to the overriding influence of local soil coverage in the studied zones on water temperature, surpassing the impact of water residence time.
- Although deeper pipe burial could partially reduce the water temperature in the pipes, it is not necessarily a comprehensive solution to eradicate the water warming problem during hot periods. This is especially the case in systems with highly mineralized surfaces and systems depending on surface water sources as these sources have inherently higher source temperatures compared to underground sources during hot periods.
- The efficacy of urban greening in moderating drinking water temperature was noteworthy. It should be noted that greening should be done in a certain pipe length to be effective.

Water temperature modeling is a powerful decision-making tool for monitoring water temperature variations within cities. Notably in the absence of extensive data and resources for direct water temperature monitoring, water utilities can benefit from the proposed approach for improved water quality management. Looking forward, it is recommended to assess the repercussions of the observed temperature disparities on microbial and chemical water quality within the DWDS.

CRediT authorship contribution statement

Faezeh Absalan: Conceptualization, Data curation, Formal analysis, Methodology, Software, Validation, Visualization, Writing – original draft, Writing – review & editing. **Fatemeh Hatam:** Software, Validation, Writing – review & editing, Investigation. **Mirjam Blokker:** Methodology, Software, Validation, Writing – review & editing. **Marie-Claude Besner:** Writing – review & editing. **Michèle Prévost:** Conceptualization, Formal analysis, Funding acquisition, Project administration, Resources, Supervision, Writing – review & editing. **Françoise Bichai:** Conceptualization, Funding acquisition, Investigation, Project administration, Resources, Supervision, Writing – review & editing.

Declaration of competing interest

The authors declare no conflict of interest. The funders had no role in the design of the study; in the collection, analyses, or interpretation of data; in the writing of the manuscript, or in the decision to publish the results.

Data availability

Data will be made available on request.

Acknowledgement

The authors would like to thank the staff of the drinking water chair in Polytechnique Montreal, especially Mr. Yves Fontaine for his valuable cooperation during the monitoring campaign. We would also like to extend our appreciation to the City of Montreal for providing the information, resources, and permission for the sampling campaign. Additionally, our thanks go to Bentley Water Systems for granting access to the unlimited version of WaterGEMS (10.04.00.108). This project was funded by the NSERC Discovery Grant of the last author, Polytechnique's half-stipends for doctoral research, and the NSERC grant, ALLRP 545363-19, from the Industrial Chair on Drinking Water in Polytechnique Montreal.

Supplementary materials

Supplementary material associated with this article can be found, in the online version, at doi:10.1016/j.watres.2024.121490.

References

Agudelo-Vera, C., Avvedimento, S., Boxall, J., Creaco, E., De Kater, H., Di Nardo, A., Djukic, A., Douterelo, I., Fish, K.E., Rey, P.L.I., 2020. Drinking water temperature around the globe: understanding, policies, challenges and opportunities. Water 12, 1049.

Agudelo-Vera, C., Blokker, M., van der Wielen, P., Raterman, B., Dorland, E., 2015. Drinking Water Temperature in Future Urban Areas. KWR Nieuwegein, The Netherlands.

Agudelo-Vera, C.M., Blokker, M., de Kater, H., Lafort, R., 2017. Identifying (subsurface) anthropogenic heat sources that influence temperature in the drinking water distribution system. Drink. Water Eng. Sci. 10, 83–91.

Alexander, C., 2021. Influence of the proportion, height and proximity of vegetation and buildings on urban land surface temperature. Int. J. Appl. Earth Obs. Geoinf. 95, 102265.

Blokker, E.M., Pieterse-Quirijns, E., 2013. Modeling temperature in the drinking water distribution system. J.-Am. Water Works Assoc. 105, E19–E28.

Donneesquebec (2019), https://www.donneesquebec.ca/recherche/dataset/vmtl-ilots-de-chaleur.

Edan, M.H., Maarouf, R.M., Hasson, J., 2021. Predicting the impacts of land use/land cover change on land surface temperature using remote sensing approach in Al Kut. Iraq. Phys. Chem. Earth 123, 103012. Parts A/B/C.

Estrada-Calderon, G., Becerra-Santacruz, H., 2022. Temperature sensitive surface to minimize the urban heat island effect. In: 2022 7th International Conference on Smart and Sustainable Technologies (SpliTech). IEEE, pp. 1–5.

Frie, E., Gilmer, S., Buraga, B., Franceschini, K., 2022. Quantifying the albedo of the montreal island and its potential for increase. McGill Sci. Undergraduate Res. J. 17, 38–44.

Kafy, A.-A., Al Rakib, A., Fattah, M.A., Rahaman, Z.A., Sattar, G.S., 2022. Impact of vegetation cover loss on surface temperature and carbon emission in a fastest-growing city, Cumilla, Bangladesh. Build. Environ. 208, 108573 https://doi.org/10.1016/j.buildenv.2021.108573.

Kimbrough, D.E., 2019. Impact of local climate change on drinking water quality in a distribution system. Water Qual. Res. J. 54, 179–192.

Kreitmair, M.J., Makasis, N., Bidarmaghz, A., Terrington, R.L., Farr, G.J., Scheidegger, J. M., Choudhary, R., 2020. In: Effect of anthropogenic heat sources in the shallow subsurface at city-scale, E3S web of conferences. EDP Sciences, p. 07002.

Lai, Y., Dzombak, D.A., 2021. Assessing the effect of changing ambient air temperature on water temperature and quality in drinking water distribution systems. Water 13, 1916.

Leveque, B., Burnet, J.-B., Dorner, S., Bichai, F., 2021. Impact of climate change on the vulnerability of drinking water intakes in a northern region. Sustain. Cities Soc. 1–22. https://doi.org/10.1016/j.scs.2020.102656.

Machell, J., Boxall, J., 2014. Modeling and field work to investigate the relationship between age and quality of tap water. J. Water Resour. Plann. Manage. 140, 04014020.

Menberg, K., Bayer, P., Zosseder, K., Rumohr, S., Blum, P., 2013. Subsurface urban heat islands in German cities. Sci. Total Environ. 442, 123–133.

National Academies of Sciences, Engineering, and Medicine (NASEM), 2019. Management of *Legionella* in Water Systems. The National Academies Press, Washington, DC, USA.

Quebec Government (2023) Guide de bonnes pratiques d'exploitation des installations de distribution d'eau potable. https://www.environnement.gouv.qc.ca/eau/potable/installation/documents/guide-bonnes-pratiques-exploitation-install-dist-eau-potable.pdf.

Ranagalage, M., Wang, R., Gunarathna, M., Dissanayake, D., Murayama, Y., Simwanda, M., 2019. Spatial forecasting of the landscape in rapidly urbanizing hill stations of South Asia: a case study of Nuwara Eliya, Sri Lanka (1996–2037). Remote Sens. 11, 1743.

Smith, I.A., Fabian, M.P., Hutyra, L.R., 2023. Urban green space and albedo impacts on surface temperature across seven United States cities. Sci. Total Environ. 857, 159663.

Stewart, I.D., Oke, T.R., 2012. Local climate zones for urban temperature studies. Bull. Am. Meteorol. Soc. 93, 1879–1900.

Tarnawski, V., Momose, T., McCombie, M., Leong, W., 2015. Canadian field soils III. Thermal-conductivity data and modeling. Int. J. Thermophys. 36, 119–156.

Wang, J., Meng, Q., Zou, Y., Qi, Q., Tan, K., Santamouris, M., He, B.-J., 2022. Performance synergism of pervious pavement on stormwater management and urban heat island mitigation: a review of its benefits, key parameters, and co-benefits approach. Water Res. 221, 118755.

Zhu, W., Sun, J., Yang, C., Liu, M., Xu, X., Ji, C., 2021. How to measure the urban park cooling island? A perspective of absolute and relative indicators using remote sensing and buffer analysis. Remote Sens. 13, 3154.